Nuclear Physics B98 (1975) 189–203

DOUBLE POMERON EXCHANGE AND DIFFRACTIVE DISSOCIATION IN THE REACTION $pp \to pp\pi^+\pi^-$ AT 69 GeV/c

France–Soviet Union Collaboration

D. DENEGRI, J. DERRE, M.A. JABIOL. S. OTWINOWSKI * and E. PAULI
Departement de Physique des Particules Elémentaires, CEN-Saclay, France

P.F. ERMOLOV, E.P. KISTENEV, A.M. MOISEEV and M.N. UCHANOV
Institute for High Energy Physics, Serpukhov, USSR

H. BIALKOWSKA **, H. BLUMENFELD, J. LOSKIEWICZ *** and Nguyen Huu KHANH
LPNHE, Université Paris VI, France

E.G. BOOS and L.A. SANKO
Institute for High Energy Physics, Alma Ata, USSR

Received 14 April 1975

We investigate the main features of the reaction $pp \to pp\pi^+\pi^-$ at 69 GeV/c from data obtained in the Mirabelle bubble chamber at Serpukhov. A search for a double pomeron exchange mechanism contribution leads to an upper limit of $\simeq 20$ μb for $M(\pi^+\pi^-) \leqslant 0.7$ GeV under reasonable assumptions. The four-body final state is dominated by proton diffractive dissociation $p \to p\pi^+\pi^-$ (mostly $\Delta^{++}\pi^-$). The cross section for this process, as well as the t production slope and the decay distributions (of the Δ^{++}) show little variation in comparison with lower energy data.

1. Introduction

We present an investigation of the main features of the reaction $pp \to p\pi^+\pi^-p$ at 69 GeV/c. The data have been obtained in an ~ 0.2 events/μb exposure of the large (4.5 m long) hydrogen bubble chamber "Mirabelle" to a 69 GeV/c proton beam at the Serpukhov accelerator. The beam momentum spread was $\pm 0.25\%$, and the beam contamination is negligible. The average number of beam tracks/picture

* On leave from Institute of Nuclear Research, Warsaw, Poland.
** On leave from Warsaw University, Poland.
*** On leave from Krakow University, Poland.

is 4. Events are accepted from a 2.0 m long fiducial volume insuring a minimum beam track length of $\simeq 1$ m for beam direction determination, and a minimum outgoing track length of $\simeq 1$ m. The film was scanned and digitized on about $\frac{1}{2}$ life size projections. The track matching and the geometrical reconstruction are performed by the program HYDRA. For this first Mirabelle run, track ionization information allows to separate protons from lighter particles for momenta $\lesssim 1.2$ GeV/c.

2. Data selection

To extract from the total sample of 4-prong events (2150 events) the sample of events corresponding to reaction

$$pp \to pp\pi^+\pi^- \tag{1}$$

we do not make constrained kinematical fits but use directly the measured track parameters and the ionization information. We require a proton recognized by ionization which corresponds to a lab momentum cut-off of 1.2 GeV/c; such a proton is henceforth called p_S. The equivalent momentum cut-off in the antilaboratory frame corresponds to a laboratory momentum of 27 GeV/c. A positive track of $p_{lab} \geqslant 27$ GeV/c is interpreted as a proton (henceforth called p_f); in case of two positive tracks with $p_{lab} \geqslant$ GeV/c (3%), the fastest one is taken as a proton. Such a selection seems a priori to strongly bias the data. However, as it will be seen, the data are entirely dominated by proton diffractive dissociations $p \to p\pi^+\pi^-$, and a Monte Carlo simulation of the projectile proton fragmentation shows that the fraction of events with π^+ having a larger laboratory momentum than the associated proton is small ($\lesssim 15\%$), and entirely negligible for $p_{lab} \geqslant 27$ GeV/c. This kinematical feature comes from the proton-pion mass difference and is insensitive to the details of the diffraction fragmentation model. This property gives us confidence in assigning the p/π^+ interpretation to fast positive tracks.

To extract events corresponding to $pp \to p_f p_s \pi^+\pi^-$ from the sample of 524 4-prong events with a recognized proton (p_s) of $p_{lab} \leqslant 1.2$ GeV/c and at least one fast positive track of $p_{lab} \geqslant 27$ GeV/c (p_f), we use the (measured) transverse momentum balance and missing mass cuts.

Fig. 1a shows the scatter plot of the missing transverse momentum $p_t^{missing}$ *versus* the overall missing mass squared MM^2 for the sample of 4 prong events interpretable as $pp \to p_f p_s \pi^+\pi^- + n\pi^0$ ($n \geqslant 0$). Events corresponding genuinly to reaction (1) show up clearly as a marked accumulation in the lower center part of the diagram. In the region $p_t^{missing} < 200$ MeV/c, the MM^2 distribution (shaded part in fig. 1c) has the typcial shape for a sample of 4C fits. The $p_t^{missing}$ distribution (fig. 1b) peaks at $\simeq 70$ MeV/c, has a dip around 200 MeV/c and a broad secondary peak at ~ 350 MeV/c We attribute the first peak to genuine 4C fits and the second to $n\pi^0$ ($n \geqslant 1$) events. The shaded area in fig. 1b corresponds to events with $-0.2 \leqslant MM^2 \leqslant 0.03$ GeV^2; this sample is obviously enriched in 4C fit candidates and their association with the

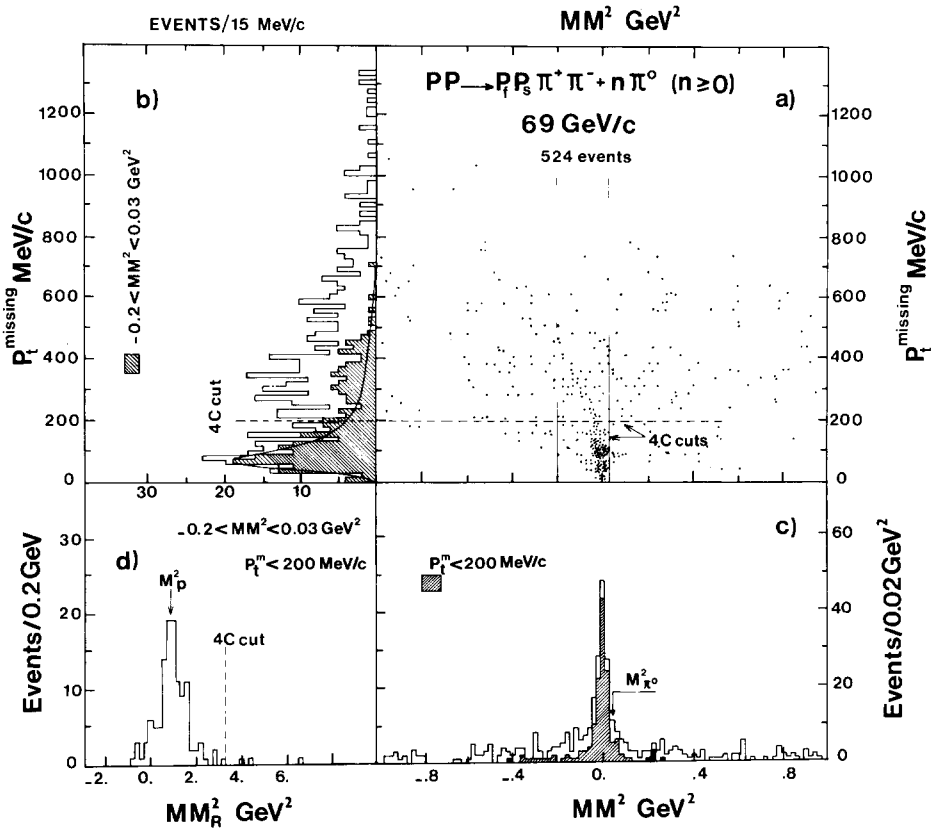

Fig. 1. (a) Scatter plot of missing transverse momentum p_t^{missing} *versus* the missing mass squared MM^2, for all four prong events with a recognized proton (p_s) and a fast positive track of $\geqslant 27$ GeV/c (p_f). Also shown are the kinematical cuts applied to extract the sample of 4C fits. (b) The p_t^{missing} projection; the shaded area corresponds to events with $-0.2 \leqslant MM^2 \leqslant 0.03$ GeV^2. The curve is explained in the text. (c) The MM^2 projection; the shaded area corresponds to events with $p_t^{\text{missing}} < 200$ MeV/c. (d) The missing mass squared MM_R^2 to the $p_s\pi^+\pi^-$ system for $p_f p_s \pi^+\pi^-$ candidate events.

peak at $p_t^{\text{missing}} \sim 70$ MeV/c is evident. A Monte Carlo simulation of $pp \to pp\pi^+\pi^-$ at 69 GeV/c events as measured in the chamber, taking into account the estimated setting error ($\epsilon = 600\ \mu$), with event vertices distributed along the fiducial volume leads us to expect the missing transverse momentum distribution shown by the full curve in fig. 1b. On the basis of fig. 1b we select our candidates to reaction (1) as $p_t^{\text{missing}} \leqslant 200$ MeV/c and $-0.2 \leqslant MM^2 \leqslant 0.03$ GeV^2. For the sample of so selected $p_f p_s \pi^+\pi^-$ candidates, fig. 1d shows the missing mass squared MM_R^2 recoiling against the (slow proton, π^+, π^-) system. The distribution is centered on M^2_{proton}, the small excess on the high mass tail is eliminated with a cut $MM_R^2 \leqslant 3.3$ GeV^2. After

these $p_t^{missing}, MM^2, MM_R^2$ cuts we are left with 123 events we attribute to reaction (1). After correction for background ($\simeq 10\%$) and losses ($\simeq 20\%$) induced by the $p_t^{missing}, MM^2, MM_R^2$ cuts, this corresponds to a cross section of $(690 \pm 70)\mu b$ for $pp \to p_f p_s \pi^+ \pi^-$ with $p_f \geqslant 27$ GeV/c, $p_s \leqslant 1.2$ GeV/c. The error is statistical, and takes into account our estimate of background and losses; the scanning loss of short recoil protons has been corrected for assuming an exponential t_{pp_s} distribution of slope 10 GeV^{-2} (see discussion in subsect. 3.2).

The largest measuring error in our data is on the momentum of the fast tracks (80% of $p_f p_s \pi^+ \pi^-$ events have $p_f \geqslant 50$ GeV/c) and are typically a few GeV/c for the fastest tracks ($p \simeq 69$ GeV/c). As we do not make kinematic fits, we partially compensate for this by recalculating, for our final sample of data, the fastest particle momentum so as to satisfy longitudinal momentum conservation.

3. Main features of the data

The principal features of reaction (1) at our energy are evident from the π^+ *versus* π^- center-of-mass rapidity plot y_{π^+} *versus* y_{π^-} (with $y = \frac{1}{2} \ln [(E + p_L)/(E - p_L)]$) shown in fig. 2a. The data exhibit a striking correlation whereby both pions tend to be simultaneously either in the forward or in the backward hemisphere. Such kinematical configurations are most naturally associated with the $N \to N\pi\pi$ diffraction dissociation diagrams in figs. 3a and b. The two quadrants (fig. 2a) corresponding to pions going in opposite hemispheres, where we expect a contribution from reaction $pp \to \Delta^{++}\Delta^0$ for example, are almost totally depopulated (12% of the data). The few events found in these regions may just be tails from the dominant diffraction dissociation mechanism. We also show in figs. 2b and 2c the p_f and p_s center-of-mass rapidity distributions (and the proton rapidity kinematical limits), separately for the forward and backward going $N\pi\pi$ clusters, defined respectively by $y_{\pi^+} + y_{\pi^-} \geqslant 0$ and $y_{\pi^+} + y_{\pi^-} \leqslant 0$.

We note that the symmetry of the initial pp state implies symmetry (within statistics) of the experimental distributions in fig. 2 with respect to the center-of-mass median plane (dashed diagonal in fig. 2a). The experimental resolution and biases are however quite different for the two hemispheres. For example the $y_{p_f}^{cm}$ distribution in fig. 2c is more degraded than the corresponding $y_{p_s}^{cm}$ in fig. 2a, and we have 68 events in the backward hemisphere as opposed to 55 in the forward one. The scanning loss of short recoil protons associated with diagram 3a for $t_{pp_s} \leqslant 0.04$ GeV^2 is estimated at 15 ± 5 events; no similar loss exists for fast protons corresponding to diagram 3b.

That the $p \to p\pi^+\pi^-$ diffractive dissociation mechanism dominates reaction (1) at our energy is also manifest from the $M^2(p_f\pi^+\pi^-)$ *versus* $M^2(p_s\pi^+\pi^-)$ scatter plot shown in fig. 4. The strong threshold enhancements in both the $M(p_f\pi^+\pi^-)$ and $M(p_s\pi^+\pi^-)$ spectra are the empirical signature allowing us to attribute the data respectively to projectile and target proton fragmentation according to diagrams a

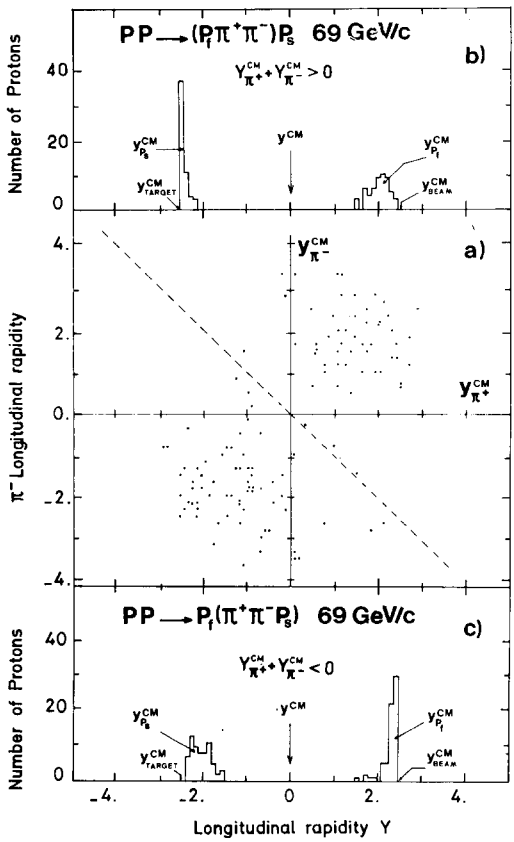

Fig. 2. (a) The π^+ *versus* π^- longitudinal rapidity plot for all pp → $p_f p_S \pi^+ \pi^-$ events at 69 GeV/*c*. (b) The p_f and p_S rapidity distributions for events in the projectile fragmentation sector defined as $y_{\pi^+} + y_{\pi^-} \geq 0$. (c) Same as in (b) but for the target proton fragmentation sector defined as $y_{\pi^+} + y_{\pi^-} \leq 0$. All rapidities are defined in the overall center of mass.

and b in fig. 3. These diffractive enhancements are studied in the second section. In the first section we turn to the question whether there is in reaction (1) a "central emission" component, which could be due to a double pomeron exchange mechanism (DPE) represented by the diagram in fig. 3c.

3.1. Search for a double pomeron exchange (DPE) contribution

A contribution from a double pomeron exchange mechanism to high energy processes is a subject of considerable theoretical interest [1–3] and is actively investigated experimentally. Lower energy experiments [4,5] give no evidence for

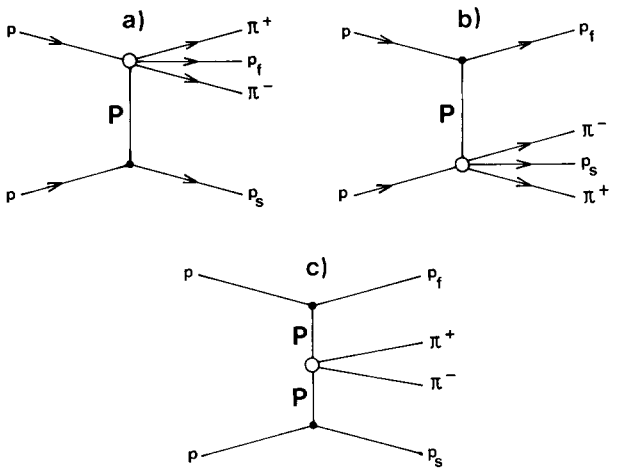

Fig. 3. (a, b) Diffraction dissociation diagrams for pp → p(pπ⁺π⁻). (c) The double pomeron exchange diagram for pp → p(π⁺π⁻)p.

a DPE contribution; recent experiments on $\pi^- p \to \pi^- \pi^+ \pi^- p$ and $pp \to pp\pi^+\pi^-$ at 200 GeV/c [6, 7] give upper limits of, respectively, $(30 \pm 11)\mu b$ and $(44 \pm 15)\mu b$, the latter value, obtained for $p\pi$ masses >2 GeV and no limitation on $\pi\pi$ masses, reduces however to 9 μb for $M(\pi\pi) \leqslant 0.6$ GeV [7].

The possibility of a DPE contribution to reaction $pp \to p(\pi^+\pi^-)p$ is based on the fact that the $\pi^+\pi^-$ effective mass (fig. 5) is strongly enhanced in the near-threshold region. We may therefore expect the $\pi^+\pi^-$ system in the region $M(\pi^+\pi^-) \leqslant 0.7$ GeV (below the ρ) to be predominantly in an S-wave $I = 0$ state, which may couple to the double pomeron as in diagram 3c. The decay angular distributions of the $\pi^+\pi^-(M(\pi\pi) \leqslant 0.7$ GeV) system, in the $\pi^+\pi^-$ rest frame with z axes along the exchanged pomeron direction, and the x-axis in the plane containing P_{inc} and P_f are indeed consistent with isotropy (fig. 6) indicating a strong S-wave component in the $\pi\pi$ system.

Fig. 7a shows the π^+ *versus* π^- center of mass rapidity plot $Y^{\text{cm}}_{\pi^+}$ *versus* $Y^{\text{cm}}_{\pi^-}$ for $pp \to p_f(\pi^+\pi^-)p_s$ events with $M(\pi^+\pi^-) \leqslant 0.7$ GeV (henceforth we call this $\pi\pi$ system the "ϵ"). The DPE contribution clearly cannot be large as we expect this mechanism to be largest around $Y_{\pi^+} \simeq Y_{\pi^-} \simeq 0$ i.e. at the center of the plot, while the data still exhibit the same forward–backward correlation noticed for the overall data (fig. 2). For a more quantitative estimate of the cross section for $\pi^+\pi^-$ production by a DPE mechanism, we compare the data in fig. 7 to the DPE model predictions. The DPE diagram is parametrized as follows:

$$A_{\text{DPE}} = \beta_{p\mathbb{P}p_f}(t_{pp_f})(S_{p_f\pi\pi})^{\alpha_{\mathbb{P}}(t_{pp_f})} F(t_{pp_f}, t_{pp_s}, M_{\pi\pi}, \Omega_{\pi\pi}) \times \beta_{p\mathbb{P}p_s}(t_{pp_s})(S_{p_s\pi\pi})^{\alpha_{\mathbb{P}}(t_{pp_s})} \quad . \tag{2}$$

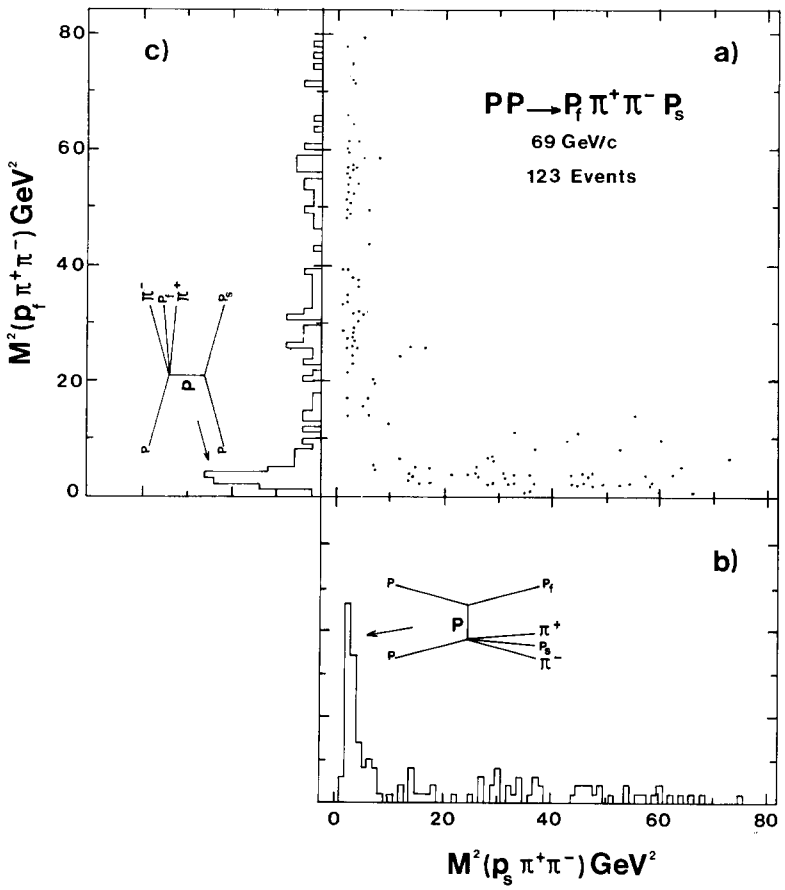

Fig. 4. Scatter plot with projections of the effective mass squared $M^2(p_f\pi^+\pi^-)$ *versus* $M^2(p_s\pi^+\pi^-)$ for all events consistent with $pp \to p_s p_f \pi^+\pi^-$. The insertions indicate the diffractive dissociations diagrams to which the threshold enhancements are ascribed.

The variables are:

$$t_{pp_f} \equiv (p_{inc} - p_f)^2 , \qquad t_{pp_s} \equiv (p_{tgt} - p_s)^2 ,$$

$$S_{p_f\pi\pi} \equiv (p_f + p_{\pi^+} + p_{\pi^-})^2 , \qquad S_{p_s\pi^+\pi^-} \equiv (p_s + p_{\pi^+} + p_{\pi^-})^2 ,$$

$\Omega_{\pi\pi}$ is the $\pi\pi$ scattering angle. In the Monte Carlo calculation the $\pi\pi$ system has been parametrized as an S-wave Breit–Wigner with $M_0 = 500$ MeV, $\Gamma_0 = 300$ MeV (the "ϵ"). The pomeron trajectories $\alpha_{I\!P}(t)$ in (2) are taken as fixed poles $\alpha_{I\!P}(t) = 1.0$. The residues $\beta_{pI\!Pp}(t)$ are taken in the form $\exp(\frac{1}{2}\gamma_p t_{pp})$ with $\gamma_p = 5$ GeV^{-2}, which

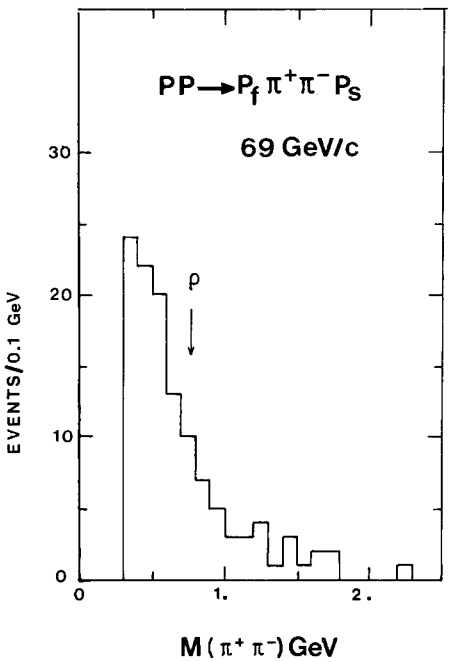

Fig. 5. The $\pi^+\pi^-$ effective mass for the reaction $pp \to p_f p_s \pi^+\pi^-$ at 69 GeV/c.

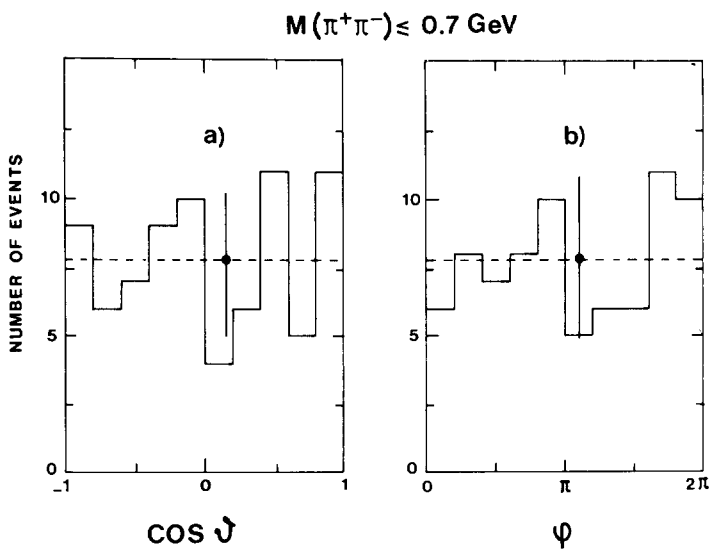

Fig. 6. (a, b) Polar (θ) and azimuthal (φ) decay angular distributions for the low mass $\pi^+\pi^-$ system ($M_{\pi\pi} \leq 0.7$ GeV). The reference frame is chosen in the $\pi^+\pi^-$ center of mass with the z axis along the p_{inc} to p_{f} momentum transfer and the x axis is in the plane containing p_{inc} and p_{f}.

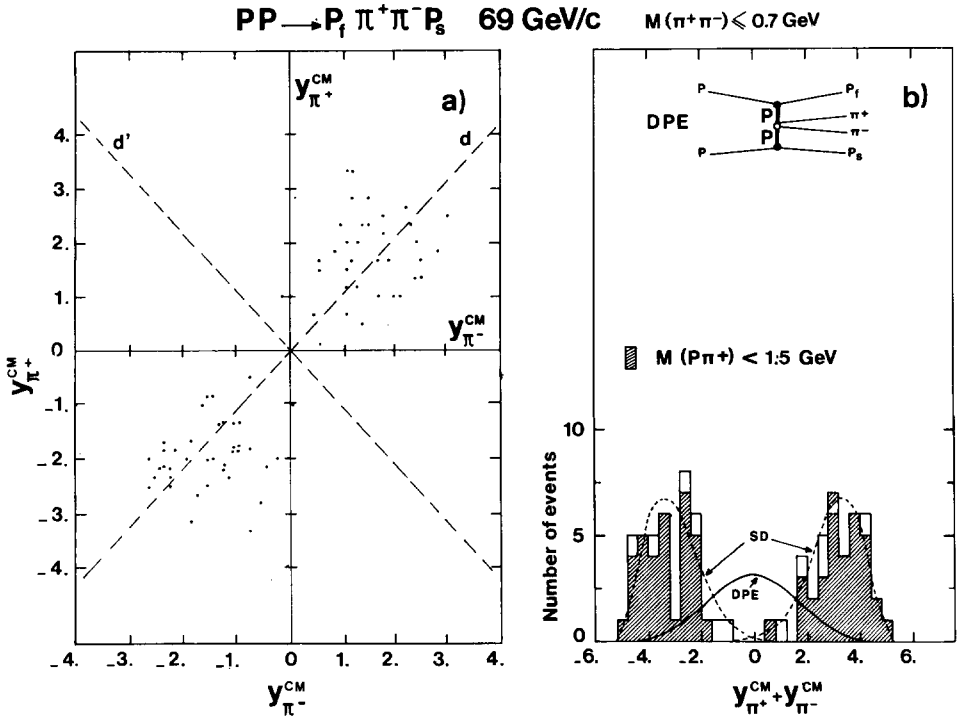

Fig. 7. (a) The π^+ *versus* π^- longitudinal rapidity for $M(\pi^+\pi^-) \leqslant 0.7$ GeV events from $pp \to p_f\pi^+\pi^- p_s$ at 69 GeV/*c*. All rapidities are defined in the overall center of mass. (b) The $y_{\pi^+} + y_{\pi^-}$ projection for same data as in (a). The shaded area corresponds to events with $M(p\pi^+) < 1.5$ GeV. The solid curve is the DPE model prediction (shown in the insert) and the dashed curve the single diffractive dissociation (SD) model prediction; for details see the text.

is obtained from the pp → pp elastic scattering slope at the same energy [8], assuming, of course, pomeron dominance and factorization for the elastic process. The unknown pomeron-pomeron-$\epsilon(\pi\pi)$ coupling function F is taken as a constant.

The model prediction is compared to the $y_{\pi^+} + y_{\pi^-}$ projection in fig. 7b (full curve, arbitrary normalization), since the most sensitive variable is obviously $y_{\pi^+} + y_{\pi^-}$. The DPE mechanism contribution is strongest around $y_{\pi^+} + y_{\pi^-} \simeq 0$ and is in sharp disagreement with the data, the central region being totally depleted. We note that the model predictions are insensitive to the details of the parametrization. In particular, they are insensitive to the parametrization of the "ϵ", to a pomeron trajectory slope of up to $\simeq 0.5$ GeV^{-2} and to moderate variations in γ_p ($4.0 \leqslant \gamma_p \leqslant 6.0$ GeV^{-2}). To estimate the maximum possible DPE contribution in the central region of fig. 7b, we evaluate the fall-off due to the dominant single dissociation (SD) mechanism, parametrizing it as follows:

$$A_{SD} = \beta_{pMp_f}(t_{pp_f})\,(S_{p_f\pi\pi})^{\alpha_M(t_{pp_f})} F_\epsilon \beta_{p\mathbb{P}p_s}(t_{pp_s})(S_{p_s\pi\pi})^{\alpha_{\mathbb{P}}(t_{pp_s})}. \quad (3)$$

This corresponds to a double peripheral diagram as in fig. 3c, but with a meson exchange in one branch and a pomeron in the other and therefore effectively reduces to the diffractive dissociation diagram in fig. 3a. A similar parametrization is used for diagram 3b. In amplitude (3) the meson trajectory is taken as $\alpha_M(t) = 0.3 + 1.0 \times t$, the pomeron as $\alpha_{\mathbb{P}}(t) = 1.0$. The residues are parametrized as follows: $\beta_{pMp}(t_{pp_f}) = \exp(\frac{1}{2}\gamma_M t_{pp_f})$ with $\gamma_M = 1.0\ \mathrm{GeV}^{-2}$ to give a small "leading particle" characteristic to the p_f (in fig. 3a), and $\beta_{p\mathbb{P}p_s}(t_{pp_s}) = \exp(\frac{1}{2}\gamma_{\mathbb{P}} t_{pp_s})$ with $\gamma_{\mathbb{P}} = 10\ \mathrm{GeV}^{-2}$ which is the slope we observe experimentally in our data for the diffractive component.

The prediction of the SD model is shown in fig. 7b (dashed curve) and clearly provides a good qualitative description of the data especially for events which have a $p\pi^+$ mass less than 1.5 GeV (shaded area on the figure). The SD model predictions are rather insensitive to moderate parameter variations: to the $\alpha_M(0)$ intercept varying from −0.2 to +0.4, to $0 \leqslant \gamma_M \leqslant 3\ \mathrm{GeV}^{-2}$ and to $7 < \gamma_{\mathbb{P}} \leqslant 12\ \mathrm{GeV}^{-2}$. Our data in fig. 7b are clearly consistent with no contribution from the DPE mechanism. To obtain an upper limit, we may in a first step attribute to DPE the three events (non Δ^{++}, i.e. $M(p\pi^+) \geqslant 1.5$ GeV) in the central region: $-1.6 \leqslant y_{\pi^+} + y_{\pi^-} \leqslant 1.6$; normalising to these the DPE model prediction, we arrive at an upper limit of 24 μb *. With the somewhat stronger requirement of $M(p\pi^+) \geqslant 1.5$ GeV and $M(p\pi^+\pi^-) \geqslant 2.0$ GeV we are left with two events and an upper limit of 16 μb. Finally, a maximum likelihood fit to the data in fig. 7b of a superposition of SD and DPE contributions indicated in fig. 7b is consistent with zero DPE and a two-standard deviation upper limit of 19 μb. We may therefore conclude at an upper limit of $\simeq$20 μb for the DPE contribution to reaction (1) with $M(\pi^+\pi^-) \leqslant 0.7$ GeV, this limit depending somewhat on the exact selections made. We note that these estimates are not affected by our experimental cuts on p_s and p_f. This can be seen from the p_f and p_s momentum distributions expected from diagram 3c parametrized following amplitude (2) and shown in figs. 8a, b (dash-dotted lines). We also note that our value is noticeably lower than the theoretically expected value of $\simeq$40 μb [3].

3.2. Study of the diffraction dissociation component

As already seen in figs. 2, 4 and 7, the reaction $pp \to pp\pi^+\pi^-$ is dominated by $p \to p\pi^+\pi^-$ diffractive dissociation. Fig. 9a shows the $p\pi^+\pi^-$ fragmentation spectrum, for the target proton fragmentation component selected according to $y^{cm}_{\pi^+} + y^{cm}_{\pi^-} \leqslant 0.0$ (we analyse only the target fragmentation as the effective mass resolution is better than for projectile fragmentation). For comparison we also show the $p \to p\pi^+\pi^-$ spectrum (selected again by $y_{\pi^+} + y_{\pi^-} \leqslant 0.0$) observed in the K

* We checked that events rejected by our kinematical cuts (sect. 2) would not modify this result appreciably: selecting as potential 4C fits events with $200 \leqslant p_t^{missing} \leqslant 400$ MeV/c and with same MM^2 and MM^2_R cuts as before, we have 1 additional event in the central region $-1.6 \leqslant Y_{\pi^+} + Y_{\pi^-} \leqslant 1.6$.

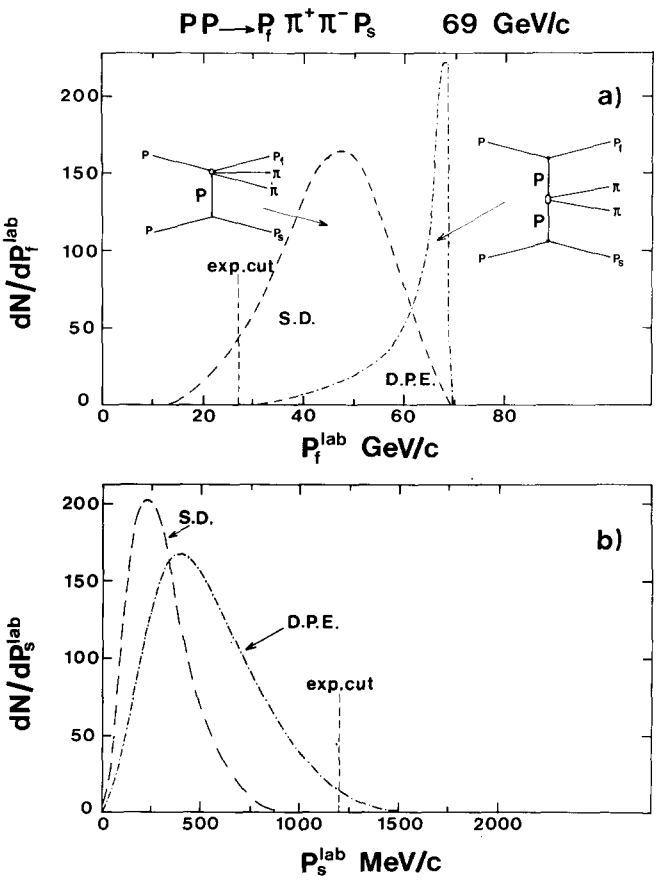

Fig. 8. Laboratory momentum spectra expected for the p_f and p_s from a $pp \to p_f p_s \pi^+\pi^-$ reaction at 69 GeV/c according to the single diffractive dissociation model (SD) and the double pomeron exchange model (DPE); also shown are the experimental cuts defining p_s and p_f.

induced reaction $K^- p \to K^-(p\pi^+\pi^-)$ at 14.3 GeV/c [9] (fig. 9a, dotted histogram). The two diffractive dissociation spectra exhibit similar shapes as expected from factorization. Figs. 9b and 9c show the $p\pi^+$ and $p\pi^-$ components of the $p_s\pi^+\pi^-$ system. The proton dissociation cluster has a dominant $\Delta^{++}\pi^-$ component, as already found at lower energies [9, 10, 11], and in a semi-inclusive study of pp interactions at 69 GeV [12], with only weak evidence for a $\Delta^0\pi^+$ subsystem. We note that for a diffractive $I = 0$ (pomeron) exchange mechanism we expect for the $I = \frac{1}{2}$ $p\pi^+\pi^- \equiv \Delta\pi$ cluster a 9 : 1 ratio of $(\Delta^{++}\pi^-) : (\Delta^0\pi^+)$ neglecting interferences. Our data are in rough agreement with such a prediction.

The $\Delta^{++}(1236)$ polar (θ) and azimuthal (φ) decay distributions, in the Δ^{++}

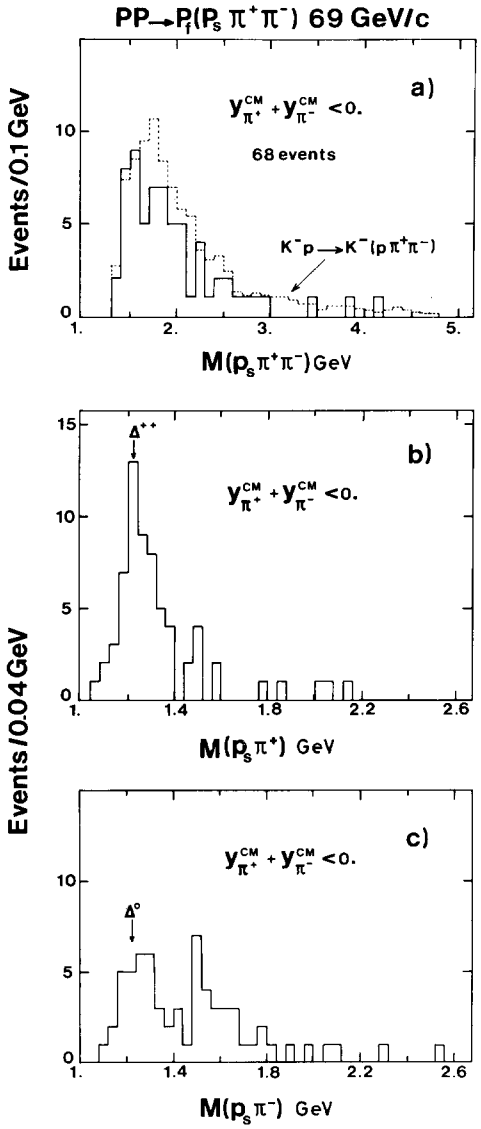

Fig. 9. (a) The $p_s\pi^+\pi^-$ effective mass for $pp \to p_f p_s \pi^+ \pi^-$ events from the target proton fragmentation sector defined as $y^{cm}_{\pi^+} + y^{cm}_{\pi^-} \leqslant 0.0$; the dotted distribution is the corresponding one from $K^-p \to K^-(p\pi^+\pi^-)$ data at 14.3 GeV/c. (b, c) The $p_s\pi^+$ and $p_s\pi^-$ effective masses for the target proton fragmentation sector.

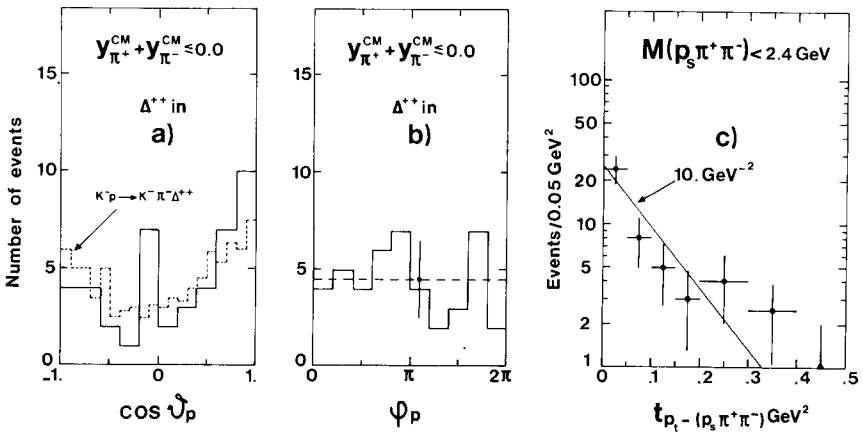

Fig. 10. (a, b) The polar (θ) and azimuthal (φ) decay distributions of the Δ^{++} from the target proton fragmentation sector. The dotted histogram in fig. 9a is the corresponding distribution from the reaction $K^-p \to K^-(\Delta^{++}\pi^-)$ at 14.3 GeV/c. (c) Momentum transfer distribution from the target proton (p_t) to the target proton fragmentation cluster ($p_s\pi^+\pi^-$) for $M(p_s\pi^+\pi^-) \leq 2.4$ GeV.

Gottfried–Jackson frame, are shown in figs. 10a and 10b. The polar distribution is compared to the corresponding one from the $K^-p \to K^-(\Delta^{++}\pi^-)$ data at 14.3 GeV/c (dotted curve, fig. 10a). The two distributions have obviously similar features.

In fig. 10c we show the production differential cross section for the $p_s\pi^+\pi^-$ cluster limited to $M(p_s\pi^+\pi^-) \leqslant 2.4$ GeV (no selection on Δ^{++}). The observed slope is $\simeq 10$ GeV^{-2}, comparable to the elastic pp slope at the same energy (10.3 ± 0.3) GeV^{-2} [8]) what supports the diffractive nature of the production mechanism. This slope is also consistent with the $pp \to p(p\pi^+\pi^-)$ production slopes at 12, 19, 24 and 205 GeV/c [10, 11, 7].

Our experimental cuts on p_s and p_f do not bias appreciably the distributions in figs. 9 and 10 as they eliminate only a small fraction of the data. This can be seen from the expected p_f and p_s lab momentum distributions for proton diffractive dissociation corresponding, for example, to diagram 3a and parametrized according to amplitude (3). For diagram 3b, which corresponds to the data in figs. 9 and 10, the conclusions are identical due to the symmetry of the initial state and the equivalence between the p_f and p_s cuts mentioned in sect. 2.

The shapes of these spectra are shown in figs. 8a and b (denoted by SD); these shapes are very insensitive to the details of the parametrization, and show that our experimental cuts in $p_s \leqslant 1.2$ GeV/c and $p_f \geqslant 27$ GeV/c result in $\simeq$15% loss of diffractive dissociation events in reaction (1).

The cross sections for $pp \to p(p\pi^+\pi^-)$ at 69 GeV/c, for a fragmentation cluster

mass $M(p\pi^+\pi^-) \leqslant 2.4$ GeV and with no background subtraction, is estimated at $(315 \pm 50)\,\mu$b (for one hemisphere). This value is corrected for the p_s and p_f experimental cuts. The equivalent production cross sections for the $p\pi^+\pi^-$ system in pp interactions at 12, 24 GeV/c [10] and 205 GeV/c [7] are, respectively, $(550 \pm 80)\,\mu$b, $(450 \pm 50)\,\mu$b and $(290 \pm 60)\,\mu$b *. The relatively slow variation of the cross section over the 12–200 GeV/c range strongly supports the diffractive nature of the production mechanism of the $N\pi\pi$ cluster. This is further supported by the most recent ISR results [13] on reaction (1) at ~1000 GeV/c and 1500 GeV/c equivalent incident momenta, yielding cross sections of respectively $(165 \pm 50)\,\mu$b and $(170 \pm 50)\,\mu$b for $M(p\pi^+\pi^-) \leqslant 2.5$ GeV (for one hemisphere). A fit of these production cross sections of the low mass $p\pi^+\pi^-$ cluster over the 12–1500 GeV/c range ** in terms of $\sigma = Ap^{-n}$ gives $n = 0.25 \pm 0.05$. This should be contrasted with the overall rate of change of the reaction $pp \to pp\pi^+\pi^-$ which is given by $p^{-0.64}$ in the 7–28 GeV/c range [7]. With the vanishing of the non-diffractive production mechanism contributions at higher energies, we may expect this rate of change to slow down and approach asymptotically the behaviour of the diffractive component.

4. Conclusions

The reaction $pp \to pp\pi^+\pi^-$ at 69 GeV/c is entirely dominated by the nucleon diffractive dissociation $N \to N\pi\pi$. The properties of the $N\pi\pi$ dissociation cluster: the mass spectrum, dominance of the $\Delta^{++}\pi^-$ substate, the Δ^{++} decay angular distributions and the $N\pi\pi$ production differential cross section, are very much the same as these observed in high statistics lower energy experiments. Furthermore, the $N\pi\pi$ cluster production cross section shows little energy variation between 12 and 200 GeV/c, supporting the diffractive nature of the production mechanism. A search for a central emission component $pp \to p(\pi^+\pi^-)p$ due to a double pomeron exchange mechanism gives no evidence for such a contribution at a level of $\lesssim 20\,\mu$b for a $\pi^+\pi^-$ mass $\leqslant 0.7$ GeV, at an incident momentum of 69 GeV/c. The lack of evidence for a DPE contribution in this study may be due to the small value of the pomeron-pomeron-ϵ coupling.

* These cross sections are estimates based on published data [4, 7, 10]. They correspond to similar definitions of the $N\pi\pi$ cluster, with minor differences however; they are all reduced to one hemisphere.

** We neglected the small difference in $p\pi^+\pi^-$ mass cuts ($\leqslant$2.5 GeV *versus* $\leqslant$2.4 GeV) applied to the 1000 and 1500 GeV/c data.

References

[1] G.F. Chew and W.R. Frazer, Phys. Rev. 181 (1969) 1914;
P.D. Ting and H.I. Yesian, Phys. Letters 35B (1971) 321.
[2] C.H. Mehta and D. Silverman, Nucl. Phys. B52 (1973) 77;
A.B. Kaidalov and K.A. Ter Martirosyan, Nucl. Phys. B75 (1974) 471.
[3] D.M. Chew and G.F. Chew, Phys. Letters 53B (1974) 191.
[4] Bonn-Hamburg-München Collaboration, Nucl. Phys. B53 (1973) 282.
[5] D. Denegri et al., Nuovo Cimento 21A (1974) 556, and references therein.
[6] D.M. Chew, Search for experimental evidence on exclusive double pomeron exchange, LBL preprint 3009.
[7] M. Derrick et al., Phys. Rev. Letters 32 (1974) 80;
M. Derrick et al., Phys. Rev. D9 (1974) 1215.
[8] France-Soviet Union Collaboration, Study of two-prong events in pp interactions at 69 GeV/c, submitted to the 17th Int. Conf. on high-energy physics, London 74, preprint M10.
[9] Saclay-Ecole Polytechnique-Rutherford Collaboration, Systematics of meson and baryon diffractive threshold enhancements, in preparation.
[10] P. Kobe et al., Nucl. Phys. B52 (1973) 109.
[11] Copenhagen-Helsinki-Oslo-Stockholm Collaboration, Nucl. Phys. B42 (1972) 558.
[12] France-Soviet Union Collaboration, Study of reactions with an identified proton in pp interactions at 69 GeV/c, submitted to the 17th Int. Conf. on high-energy physics, London 74, preprint M11.
[13] R. Webb et al., Physics Letters 55B (1975) 331.